Applied Surface Science 590 (2022) 153082

Contents lists available at ScienceDirect

Applied Surface Science

journal homepage: www.elsevier.com/locate/apsusc

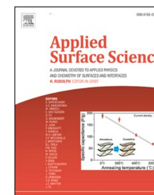

Controlling the crystallinity of HfO_2 thin film using the surface energy-driven phase stabilization and template effect

Ae Jin Lee [a], Byung Seok Kim [a], Ji Hyeon Hwang [a], Youngjin Kim [a], Hansol Oh [b], YongJoo Park [b], Woojin Jeon [a,*]

[a] *Department of Advanced Materials Engineering for Information and Electronics, and Integrated Education Program for Frontier Science & Technology (BK21 Four), Kyung Hee University, Yongin, Gyeonggi 17104, Republic of Korea*

[b] *Advanced Research Development Team, SK Trichem Co. Ltd, Sejong 30068, Republic of Korea*

ARTICLE INFO

Keywords:
Dielectric constant
Phase transition
Crystallization
Hafnium oxide
Laminated structure

ABSTRACT

Phase transition of HfO_2 thin film has been investigated to demonstrate desirable electrical properties, such as high dielectric constant or ferroelectricity, however, the most of results exhibited a limitation on enhancing the crystallinity because of employing dopant. In this study, the crystallization behavior in the thin film was investigated in the intrinsic and extrinsic aspects. In the laminated structure, highly crystallized tetragonal phased HfO_2 was obtained by controlling the layer thickness and adapting the template effect for intrinsic and extrinsic crystallization, respectively, without using dopant. Moreover, by the phase composition analysis, the dielectric constant of various crystal structures of HfO_2 thin film, tetragonal, monoclinic, and amorphous phases, were revealed using the data obtained from the real deposited thin film by atomic layer deposition process, not from the theoretical calculation.

1. Introduction

HfO_2 is the most representative high dielectric constant (k) material in the high-k metal gate applications.[1–6] However, HfO_2 has k values of a wide range due to the nature of many crystal structures.[7–9] Among them, the HfO_2 thin film deposited by the conventional thin film deposition process, such as chemical vapor deposition or atomic layer deposition (ALD), generally has the monoclinic-phase (m-phase) of relatively low k value of below 20.[10] Therefore, adopting HfO_2 into the metal–insulator-metal structured-capacitor, especially for the dynamic random access memory (DRAM) application, has been limited. In contrast to the HfO_2, the tetragonal-phase (t-phase) of ZrO_2 thin film, the highest k value crystal structure of ZrO_2, is facile to obtain from the typical thin film deposition process,[11] resulting in employing the ZrO_2 thin film as the DRAM capacitor dielectric for over decades.[12–14] However, the k value of t-phase ZrO_2 is about 40, inducing the scaling limitation on implementing the next-generation DRAM device.[14,15] Adopting other high-k material candidates, such as TiO_2 and $SrTiO_3$, has been impeded because it would induce severe leakage current property degradation.[16–22] In this regard, HfO_2 has been attracted a lot of attention again. HfO_2 has almost identical physical and chemical properties to ZrO_2.[23] Furthermore, the calculation results about that the t-phased HfO_2 thin film would exhibit a k value as high as 70 [23–25] would contribute to overcoming the limitation of the ZrO_2-based DRAM capacitor. Consequently, many studies have been reported for obtaining the t-phase of HfO_2 thin film.[26–30] However, sufficiently high crystallized t-phase of HfO_2 was not achieved contrast to the ZrO_2 thin film. Both ZrO_2 and HfO_2 have a same crystal structure of the fluorite, which is based a tetragonal structure of CaF_2. However, the fact that the radius of Zr^{4+} and Hf^{4+} was not sufficiently large to sustain the fluorite structure, inducing a distortion of crystal structure with a coordination number of cation from 8 to 7. As a result, the most stable crystal structure of ZrO_2 and HfO_2 is the monoclinic structure (m-phase), which is distorted tetragonal structure. However, in the case of the film thickness is thin, the surface energy dominantly governs the crystal structure to minimized the surface energy than that of bulk. HfO_2 thin film has different surface and bulk energy depending on the crystal structure:[31,32] the t-phase has smaller surface energy (higher bulk energy) than that of m-phase, in turn, the phase transformation occurs from t- to m-phase with increasing the thickness of thin film or grain size. The thickness, where the phase transformation occurs, is called the ‘critical thickness’. In the case of ZrO_2, the critical thickness is about 10

* Corresponding author.
E-mail address: woojin.jeon@khu.ac.kr (W. Jeon).

https://doi.org/10.1016/j.apsusc.2022.153082
Received 8 September 2021; Received in revised form 26 February 2022; Accepted 11 March 2022
Available online 19 March 2022
0169-4332/© 2022 Elsevier B.V. All rights reserved.

nm, resulting in a t-phase formation. In contrast, in the HfO_2 case, the critical thickness is only 3 nm, hence, the most of deposited HfO_2 thin film exhibits the m-phase, or monoclinic dominant tetragonal mixed phase.[33–35] In other words, obtaining the t-phase HfO_2 is inherently impossible. In this regard, various extrinsic techniques have been investigated to obtain tetragonal-only phased HfO_2 thin film. Dopants of Al [11,36,37] and Si [38] exhibited an effective phase transition result, but the crystallinity of HfO_2 thin film was decreased by the introduced dopant in the lattice, simultaneously.

Therefore, in this study, we conducted inducing t-phase transformation by adopting the inherent surface energy difference among the crystal structure of HfO_2. To achieve t-phase formation, we focused on the critical thickness. HfO_2 thin film thinner than 3 nm could form the t-phase from the calculation result. In this regard, several results about the laminated structure consisting with HfO_2 and dividing layer had been reported.[39,40] However, the thickness of 3 nm was too thin to induce crystallization. In other words, using the inherent property of HfO_2 was insufficient for the t-phase formation. Therefore, the 'template effect' was employed. The template effect is a phenomenon that the crystal structure of deposited thin film determined by that of the substrate. During the initial stage of thin film deposition, the thin film grown with a crystal structure of substrate epitaxially to reduce the interface energy. To crystallize the HfO_2 thin film below the thickness of 3 nm, we employed the template effect using ZrO_2 as the dividing layer in the laminated structure. Consequently, intrinsic (inherent phase transformation of HfO_2 depending on the thickness) and extrinsic (template effect using t-phase ZrO_2) methods were employed for inducing the t-phase HfO_2. In this regard, we deposited a laminated structure, which consisted of HfO_2 and ZrO_2, and varied the thickness of the HfO_2 layer by employing the ALD process to precisely control the layer thickness of HfO_2 under the critical thickness. Moreover, t-phase ZrO_2 thin film was employed to manipulate the HfO_2 of t-phase by the template effect from the identical lattice parameter of ZrO_2 and HfO_2. The phase composition and the electrical properties of the HfO_2 layer in the laminated structure were investigated. Finally, the dielectric constant of HfO_2 thin film of various crystal structures was revealed.

2. Experimental procedure

ZrO_2 and HfO_2 thin films were deposited by means of ALD (iOV dX1, iSAC research) using cyclopentadienyltris(dimethylamino)zirconium ($CpZr[N(CH_3)_2]_3$, CpZr), and cyclopentadienyltris(dimethylamino)fafnium ($CpHf[N(CH_3)_2]_3$, CpHf) as the Zr, and Hf precursor, respectively. The substrate consisted of 50-nm-thick TiN as a bottom electrode on a thermally oxidized (1 0 0) Si wafer. In addition, Al_2O_3 for the laminated Al_2O_3/HfO_2 structure was deposited with trimethylaluminium ($Al(CH_3)_3$, TMA) as the Al precursor. O_3 was used as the oxygen source at a concentration of 170 g/m^3. The canisters of CpZr, CpHf, and TMA were maintained at 80 °C, 110 °C, and room temperature to acquire the appropriate vapor pressures of each precursor, respectively. The deposition temperature was set to 300 °C. The laminated structure dielectrics of the ZrO_2 and HfO_2 were deposited using ALD super-cycles, which consisted of ALD sub-cycles of ZrO_2 and HfO_2 with different cycle ratios to control each thickness of the inserted HfO_2 and ZrO_2 layers. Post-deposition annealing was performed at 600 °C for 30 s under N_2 atmosphere using a rapid thermal process. To measure the electrical properties, a metal–insulator-metal (MIM) capacitor was fabricated with a top electrode which consisted of 50-nm-thick Ti and 50-nm-thick Pt film that were defined by a metal shadow mask with a 300 μm diameter hole.

The film thickness was determined by calculating the layer density, which was measured via X-ray fluorescence spectroscopy (XRF, ARL Quant'X, Thermo Scientific), which correlated with the spectroscopic ellipsometer (ESM-300, J. A. Woollam). The chemical state of the dielectric was investigated via x-ray photoelectron spectroscopy (XPS, K-Alpha+, ThermoFisher Scientific). Glancing angle incident x-ray diffraction with an incident angle of 0.5° (GA-XRD, X'pert Pro, PANalytical), and transmission electron microscopy (TEM, JEOL, JEM-2100F) were used to examine the crystal structure of the films. The electrical properties were evaluated by measuring the capacitance versus voltage and the current versus voltage characteristics using Agilent 4284 and 4155C, respectively.

3. Results and discussion

Various laminated structures of HfO_2 and ZrO_2 were deposited as shown in Fig. 1. The total thickness of HfO_2 was fixed to ~ 3 nm divided by interposed ZrO_2 layer to varying each layer thickness of HfO_2 to 0.5, 1, and 3 nm (denoting H0.5ZO, H1ZO, and H3ZO). The total ZrO_2 layer thickness was also fixed to ~ 7 nm, resulting in the total thickness of the laminated structures were almost identical to 10 nm. The actual thickness of the laminated structures is described in Table 1. The XRD analysis indicated that the crystal structure of the HfO_2 layer in the laminated structure dramatically changed with respect to the layer thickness (Fig. 2). The crystal structure of 10-nm-thick ZrO_2 and HfO_2 was investigated. As shown in Fig. 2(a), ZrO_2 and HfO_2 thin films had different phase compositions: whereas the ZrO_2 thin film had the t-phase-only crystal structure, HfO_2 exhibited peaks corresponding to m- and p-phases. This result indicates that the effect of surface energy on the crystallization in ZrO_2 and HfO_2 thin films. ZrO_2 and HfO_2 have a similar crystal structure, fluorite structure, with an almost identical lattice constant due to no difference in the ionic radii between Zr^{4+} and Hf^{4+}.[41] However, the critical thickness is quite different to 3 and 10 nm for HfO_2 and ZrO_2, respectively. Therefore, the ZrO_2 and HfO_2 thin films exhibited different crystal structures even in the same physical thickness. In this regard, m-phase peaks in the XRD of the laminated structure were regarded as derived from the m-phase of the HfO_2 layer. In other words, decreasing the peak intensity of the m-phase indicates suppressing the m-phase formation of the HfO_2 layer. The deposited HZO thin film in all the samples has a mixed crystal structure of m- and t-phases, implying that m-phase formation was not fully suppressed by limiting the layer thickness of HfO_2 under the critical thickness. However, the peak intensity ratio of m- and t-phases were significantly changed depending on the thickness of the HfO_2 layer (Fig. 2(b)). In the case of H3ZO, the m-phase was dominant as the most HfO_2 thin film deposited by ALD does. In contrast, the intensity of peaks from the m-phase was gradually decreased with decreasing the thickness of the HfO_2 layer. Eventually, the contribution from the peak of the m-phase of HfO_2 layer was almost disappeared in the case of H0.5ZO. The diffraction pattern of 2θ of 29 to 33° was deconvoluted to t- (30.6°), and m- (31.8°) phases. The ratio of t- to m-phase (t/m ratio) was significantly increased about eight times from H3ZO of 1.02 to H0.5ZO of 7.79 (Table 2). This result implies that control the layer thickness of HfO_2 is effective to suppress the m-phase formation. TEM analysis was conducted to investigate the micro-structure of the HZO films depending on the layer thickness of HfO_2 (Fig. 3). In the cases of H3ZO, the energy dispersive spectroscopy (EDX) image of Hf exhibited that the HfO_2 was located in the middle of the thin film, as depicted in the schematic structure of H3ZO (Fig. 1). For the H1ZO, the Hf was dispersed more widely, but a distinctive ZrO_2 layer between TiN and H1ZO was observed. However, HfO_2 in H0.5ZO thin film did not observed as a separate layer, and dispersed into entire H0.5ZO film as shown in EDX analysis. Moreover, the fast-Fourier-transform (FFT) patterns were obtained for all the thin films (Fig. 5). In the case of H3ZO thin film (Fig. 4(a)), the FFT patterns for the region where ZrO_2 and HfO_2 would be dominant were obtained as shown in Fig. 4(b) and 4(c), respectively. Whereas the ZrO_2 layer exhibited diffraction points only corresponding to the t-phase (Fig. 4b), a pattern from HfO_2 layer was consisted with diffraction points by the m-phase (Fig. 4c). This result implies that the m-phase diffraction peak in the XRD measurement was originated from the HfO_2 layer. In the cases of H1ZO and H0.5ZO, the FFT patterns were obtained from the whole range of the thin film (Fig. 4(d) and 4(f)) because it was hard to distinguish ZrO_2 and HfO_2 separately. In the FFT pattern of the H1ZO

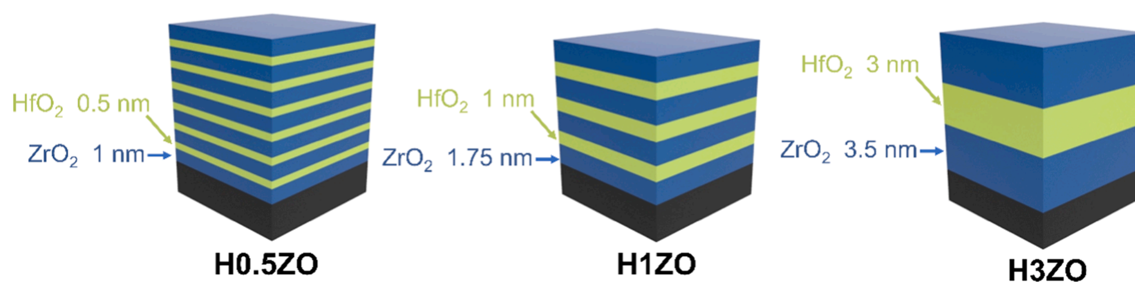

Fig. 1. Schematic diagram of the thin film stacks.

Table 1
Information on the thickness of the constituent layers of the laminated structure.

Sample	ZrO_2 thickness (nm)		HfO_2 thickness (nm)		Total laminated structure thickness (nm)
	Total	Single layer	Total	Single layer	
H0.5ZO	6.59	0.941	2.88	0.48	9.47
H1ZO	6.38	1.60	2.95	0.983	9.33
H3ZO	7.14	3.57	3.01	3.01	10.15

thin film (Fig. 4(e)), diffraction points from both t-, and m-phases were observed, but the intensity of the point corresponding to the m-phase was significantly weaker than that from the t-phase. Furthermore, the m-phase diffraction point was almost disappeared in the H0.5ZO film (Fig. 4(g)), which coincided with the XRD results. However, it was not possible to investigate whether the phase transition from m- to t-phase occurred because the diffraction corresponding to the t-phase of HfO_2 are located at the same 2θ or reciprocal lattice of ZrO_2 t-phase peaks in XRD and TEM analyses, respectively.

To clarify the t-phase formation of the HfO_2 layer, XPS measurement was employed. Since the binding energy of Hf^{4+} is changed regarding the crystal structures, the phase composition of HfO_2 layer was revealed by deconvolution of the Hf $4f_{7/2}$ peak to amorphous (17.4 eV), m- (17.9 eV), and t- (18.1 eV) phases (Fig. 5).[42] The relative phase composition was significantly changed depending on the HfO_2 layer thickness (Fig. 5 (d) and Table 2). In the case of H3ZO, the HfO_2 layer was crystallized to m-phases of a ratio of 0.83. The ratio of m-phase was dramatically decreased to 0.145 and 0.146 in H1ZO and H0.5ZO, respectively, which inferred the m-phase formation is efficiently hindered below the critical thickness. However, the suppression of the m-phase did not ensure the transformation to the t-phase. Even though the suppression behavior of

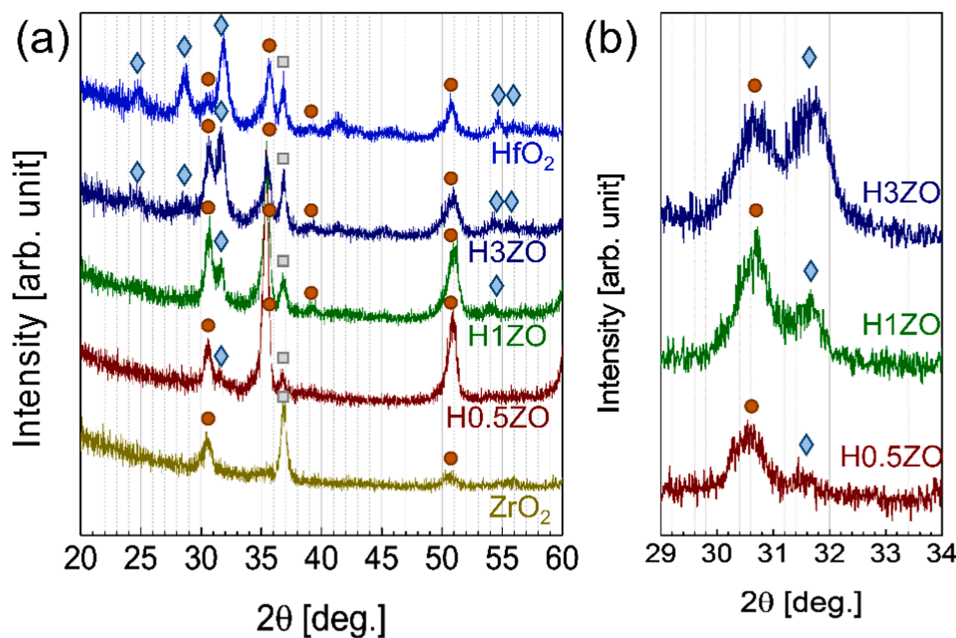

Fig. 2. (a) XRD patterns of various thin film stacks. The symbols in the pattern ◆, ●, and ■ indicates peak from monoclinic, tetragonal phases of ZrO_2 or HfO_2, and TiN substrate, respectively. (b) Magnified XRD patterns from (a). Red and blue lines were denoted the deconvolution peaks for tetragonal and monoclinic phases, respectively.

Table 2
Relative phase composition and dielectric constant of the laminated structures.

Sample	Peak area (by XRD)			Relative phase composition (by XPS)			Dielectric constant	
	t-phase	m-phase	t/m ratio	t-phase	m-phase	amorphous	Total	HfO_2
H0.5ZO	30.7	3.94	7.79	0.694	0.146	0.16	38.31	36.82
H1ZO	58.9	23.5	2.50	0.495	0.145	0.36	35.65	29.84
H3ZO	61.8	60.8	1.02	0.07	0.83	0.1	28.98	18.01

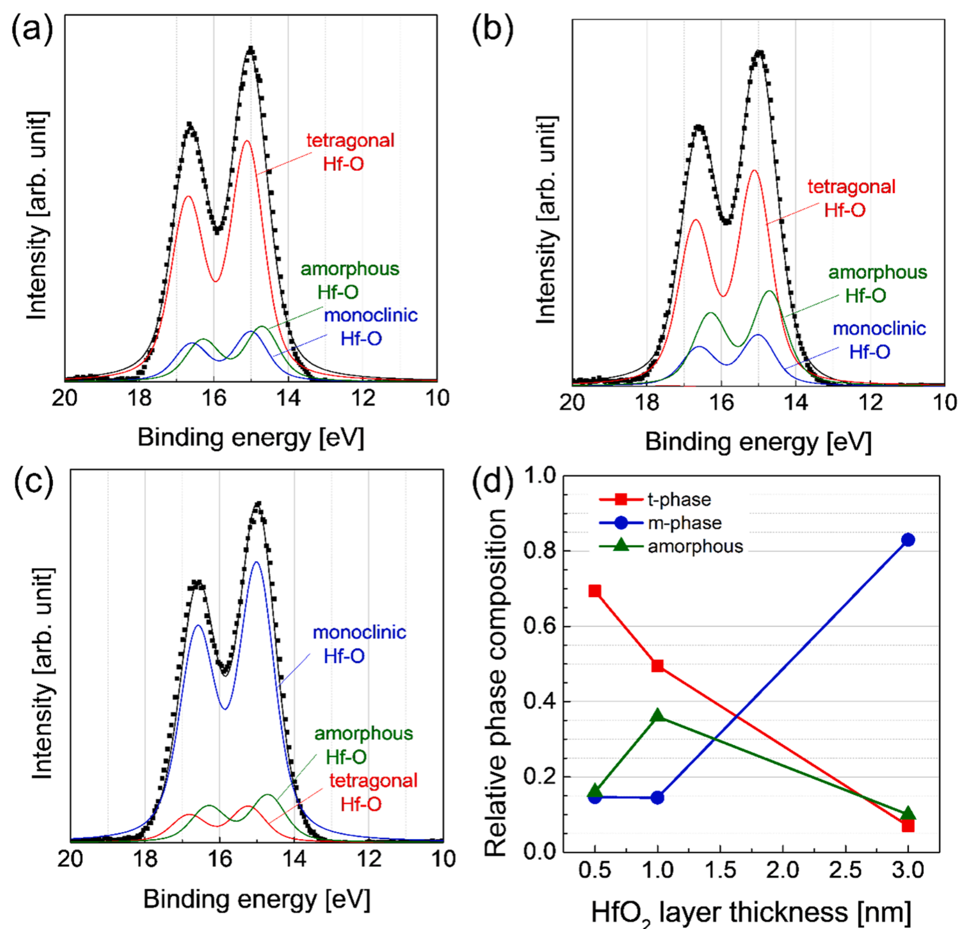

Fig. 3. (a), (d), and (g) are scanning TEM images, for H3ZO, H1ZO, and H0.5ZO, respectively. EDX images of Zr ((b), (e), and (h)) and Hf ((c), (f), and (i)) for H3ZO, H1ZO, and H0.5ZO, respectively.

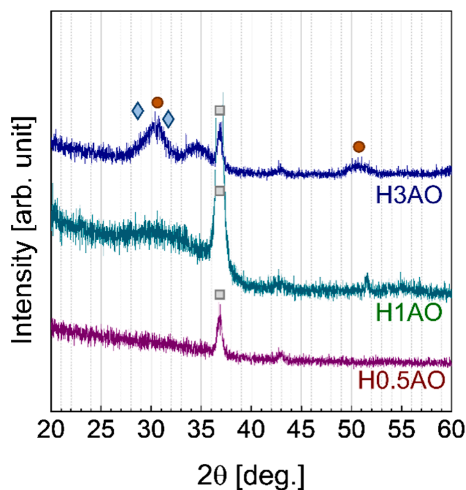

Fig. 4. (a) High-resolution TEM image of the H3ZO. FFT patterns from (b) the red box (ZrO_2 layer) in (a), and (c) the blue box (HfO_2 layer) in (a). (d) High-resolution TEM image of the H1ZO/TiN, and (e) FFT pattern from the white box in (d). (f) High-resolution TEM image of the H0.5ZO/TiN, and (g) FFT pattern from the white box in (f).

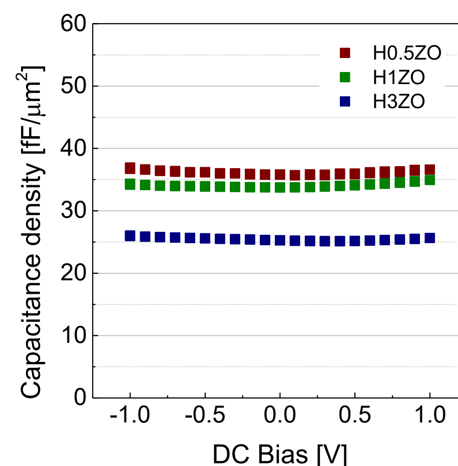

Fig. 5. Hf 4f XPS spectra of (a) H0.5ZO, (b) H1ZO, and (c) H3ZO. (d) The calculated relative phase composition from the deconvolution XPS spectra.

m-phase was observed almost identical in H1ZO and H0.5ZO, the ratio of t-phase was quite different with respect to the HfO_2 layer thickness: t-phase ratio of 0.694 and 0.495 for H0.5ZO and H1ZO, respectively. The difference in t-phase ratio was compensated by the ratio of amorphous phase difference: H1ZO had a relatively higher amorphous phase ratio of 0.36 than that of H0.5ZO of 0.16. This result indicated that suppressed m-phase formation transformed to the amorphous phase in the H1ZO case, not to transform to the t-phase which was intended. In this result, the ratio of amorphous phase should be emphasized. In the general case in the thin film deposition, the thicker layer tends to have higher crystallinity, however, thinner layer thickness (H0.5ZO) had higher crystallinity than that of thicker (H1ZO). This implies only employing

limiting the layer thickness below the critical thickness is not sufficient to induce the t-phase transformation from the m-phase of HfO_2. In this case, the crystallinity of ZrO_2, interposed between the HfO_2 layers, served as a template for the t-phase crystallization of HfO_2 layer. The ratio of surface in contact with the ZrO_2 layer decreased as the thickness of HfO_2 layer increased, resulting in increasing the ratio of amorphous phase in the HfO_2 layer. To confirm the template effect by ZrO_2 layer on the crystallization of the HfO_2 layer, the crystallinity of the laminated structure consisting with HfO_2 and Al_2O_3, oxide of the amorphous phase, with varying the HfO_2 layer thickness of 0.5, 1, and 3 nm was investigated (Fig. 6). To obtain sufficient peak intensity in the XRD measurement, the total thickness of HfO_2 layers in the sample was fixed to 15 nm. In the case of H0.5AO, no notable diffraction peak was observed. This result indicated the HfO_2 layer of 0.5 nm was too thin to crystallize without any extrinsic driving forces. The broad peak of approximately 28-35° observed in the H1AO sample indicated the *meso*-crystalline structure, which consisted of crystalline nuclei and amorphous region. In other words, the peak due to the diffraction was not observed until the thickness of HfO_2 layer was about 3 nm. A diffraction peak, which was even still too broad to distinguish the exact corresponding phase, was observed in the HfO_2 layer of 3-nm-thick. This result implies the t-phase dominant transformation in the H0.5ZO was attributed to both an intrinsic, suppressing the m-phase formation by limiting the layer thickness under the critical thickness, as well as an extrinsic attribution, inducing the t-phase crystallization caused by the template effect from the crystalline interposed ZrO_2 layer.

From the above results, the crystallization mechanism in the HfO_2 thin film was understood as below. To demonstrate the crystallization of the HfO_2 thin film by the intrinsic driving force, widely known as competition between surface energy and bulk energy of nuclei, the thin film thickness should be higher than 3-nm-thick. Up to 3 nm, the crystallized region, called grain, could not be stabilized, hence, the thin film consisted of amorphous and nuclei, as shown in the comparison between H3AO and H1AO. Moreover, m-phase formation in the H3ZO also indicates the dominant crystal structure of the thin film is governed by the intrinsic aspect, thermodynamical stable phase of thin film material itself, with a thickness 3 nm or thicker. To induce the crystallization against the intrinsic aspect, the template effect was employed generally. From the result from the H0.5ZO and H1ZO, the template effect affects about 0.5 nm-thick region.

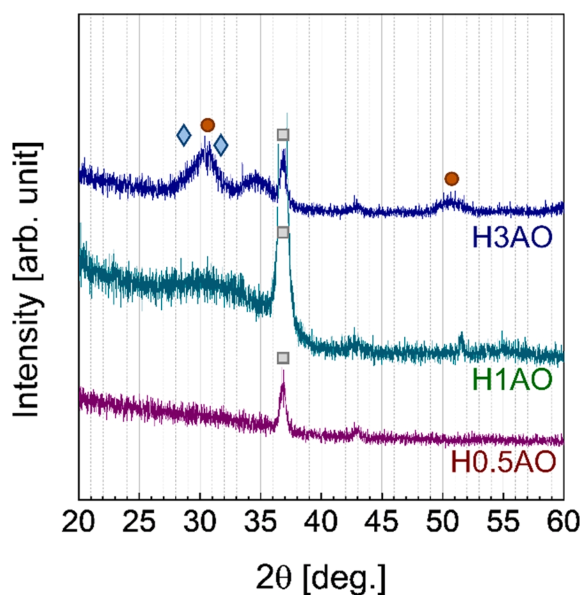

Fig. 6. XRD patterns of the thin films consisted with HfO2 and Al2O3 layers. The symbols in the pattern ◆, ●, and ■ indicates peak from monoclinic, tetragonal phases of ZrO_2 or HfO_2, and TiN substrate, respectively.

According to the crystal structure, the electrical property of each sample exhibited different characteristics. For the first, the *k* value of the laminated structures was changed by the layer thickness of HfO_2 (Fig. 7 (a) and 7(b)). The *k* value was increased with decreasing the HfO_2 layer thickness. In the case of H3ZO, the *k* value was 28.98, which was much smaller than that of the 9.6-nm-thick ZrO_2 thin film of 42.3, indicating that the m-phase formation of HfO_2 decreases the total *k* value of the laminated structure. Indeed, the *k* value of the 9.9-nm-thick HfO_2, which has the m-phase crystal structure, was 16.8. Compared to the H3ZO case, the *k* values of H1ZO and H0.5ZO increased to 35.55 and 38.31, respectively. From the *k* value of each laminated structure, the *k* value of the HfO_2 layer was calculated under the assumption that the *k* value of ZrO_2 layer was 42.3 (Table 2). Since the laminated structure can be assumed equivalent to a circuit consisted of parallel capacitors of ZrO_2 and HfO_2, the total capacitance is demonstrated by the simple equation of $1/C_{total} = 1/C_{ZrO2,1} + 1/C_{HfO2,1} + 1/C_{ZrO2,2} + 1/C_{HfO2,2} + \ldots$. From this calculation, *k* values of the HfO_2 layer were 36.82, 29.84, and 18.01 in H0.5ZO, H1ZO, and H3ZO, respectively. Notably, through the calculated *k* value, it was confirmed that the *k* value of the HfO_2 layer is substantially improved through the phase transformation from m-phase to t-phase. Furthermore, based on the results about the relative phase composition and *k* value of HfO_2 layer from three samples (Table 2), the *k* value of each phase of HfO_2 thin film was calculated. From the calculation, *k* values of t-, m-, and amorphous-phase are 46.89, 16.31, and 11.85, respectively. It should be emphasized that the *k* values were calculated based on the actual experimental results, not from the theoretical results. Actually, the *k* value of m-phase from the calculation was 16.31, which was almost identical to the *k* value of 16.8 obtained from the 9.9-nm-thick HfO_2 thin film. Moreover, the contribution of the less crystallized region at the interface or boundary on the *k* value measurement was excluded by considering the amorphous phase, separately. Consequently, it can be said that it is the result of the closest to the real value of the *k* of HfO_2 thin film in a single phase, which can obtain through the ALD process, in which some contaminants or defects are incorporated.

Additionally, the *k* value achieving the ZrO_2/HfO_2 nanolaminated structure was compared with previous results about enhancing the *k* value of HfO_2 (Table 3). The previous results also tried to demonstrate the t-phase formation and suppression of m-phase to increase the *k* value, but they employed a method of inducing the strain by using a dopant. To induce a sufficient strain achieving the phase transformation, relatively high dopant concentration was inevitable, resulting in a limitation on increasing the crystallinity and the *k* value. In contrast, the ZrO_2/HfO_2 nanolaminated structure was achieved the phase transformation of HfO_2 from monoclinic to tetragonal without using any dopant. Furthermore, the leakage current property in the ZrO_2/HfO_2 nanolaminated structure was enhanced. As shown in Fig. 7(c), the leakage current density of all the HZO thin films exhibited 1–2 orders reduced level than that of the HfO_2 thin film. Therefore, the crystallinity of HfO_2 layer was enhanced and achieving a relatively higher *k* value without any degradations in the electrical properties.

4. Conclusion

Crystallinity control of HfO_2 thin film was investigated in the laminated structure consisted of ZrO_2 and HfO_2 by using layer thickness control and induced template effect. The surface and bulk energy difference depending on the phases of HfO_2 thin film makes the suppression of the m-phase formation with decreasing the HfO_2 layer thickness. Moreover, the t-phase crystallinity of the interposed ZrO_2 induced the t-phase transformation of HfO_2 thin film by the template effect. The t-phase of HfO_2 was achieved using intrinsic (thickness below the critical thickness) as well as extrinsic (template effect) aspects. Consequently, a high *k* value of HfO_2 of 36.82 was achieved. Furthermore, based on the phase composition analysis of the thin films, the *k* values of t-, m-, and amorphous-phase were extracted to 46.89, 16.31, and 11.85,

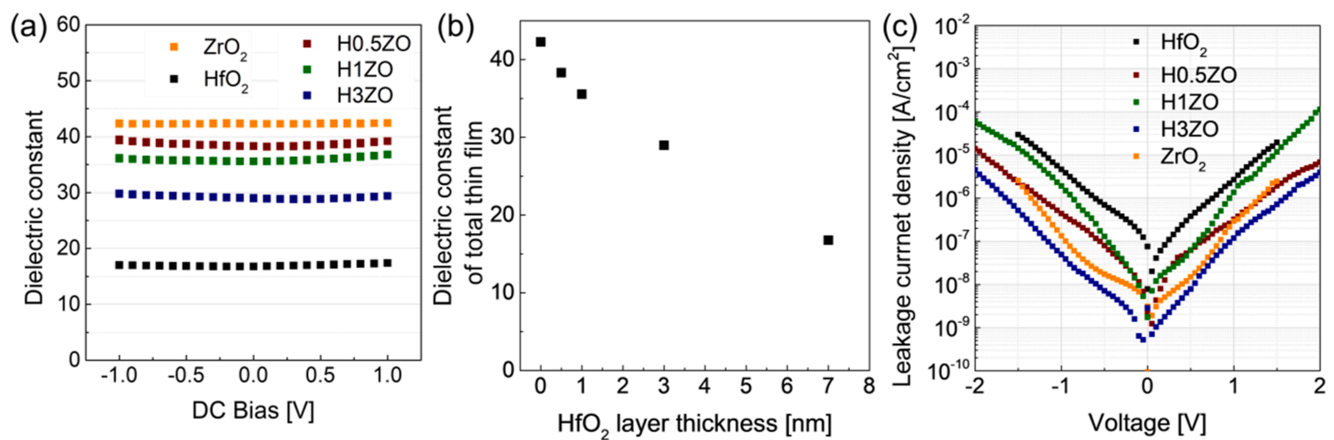

Fig. 7. (a) Dielectric constant vs. DC bias curves of the MIM capacitor with H0.5ZO, H1ZO, and H3ZO. For the comparison 9.6-nm-thick ZrO_2 and 9.9-nm-thick HfO_2 were depicted. (b) Dielectric constant of total thin film regarding the HfO_2 layer thickness from (a). (c) Leakage current density vs. voltage curves for H0.5ZO, H1ZO, H3ZO, 9.6-nm-thick ZrO_2, and 9.9-nm-thick HfO_2 thin films.

Table 3
Previous results about the dielectric constant enhancement of HfO_2 thin film.

Sample	Dielectric constant of thin film	Reference
ZrO_2/HfO_2 (*this work*)	38.31	
ZrO_2/HfO_2	35	[35]
Ce-doped HfO_2	32	[27]
Y-doped HfO_2	33.4	[43]
Al-doped HfO_2	35	[11]
	21.2	[37]
Si-doped HfO_2	27	[38]
	35	[44]

respectively. From the fact that the extracted k value was based on the actual experimental result deposited by ALD, not from the theoretical calculation, these k values implied the expected k value by employing the HfO_2 thin film to the actual devices.

CRediT authorship contribution statement

Ae Jin Lee: Conceptualization, Investigation, Writing – original draft. **Byung Seok Kim:** Investigation. **Ji Hyeon Hwang:** Visualization. **Youngjin Kim:** Conceptualization, Data curation, Writing – review & editing. **Hansol Oh:** Investigation, Resources. **Yong Joo Park:** Investigation, Resources. **Woojin Jeon:** Conceptualization, Validation, Data curation, Writing – review & editing, Supervision.

Declaration of Competing Interest

The authors declare that they have no known competing financial interests or personal relationships that could have appeared to influence the work reported in this paper.

Acknowledgement

This work was supported by the Technology Innovation Program (No. 20016813 and 20017228) funded by the Ministry of Trade, Industry & Energy (MOTIE, Korea), Basic Science Research Capacity Enhancement Project through Korea Basic Science Institute (National research Facilities and Equipment Center) grant funded by the Ministry of Education.(No. 2019R1A6C1010052), and Korea Institute of Energy Technology Evaluation and Planning (KETEP) grant funded by the Korea government (MOTIE) (20201520300140, Development of Advanced Functional Material with C-14 from PHWR Waste).

References

[1] H. Kim, A. Marshall, P.C. McIntyre, K.C. Saraswat, Crystallization kinetics and microstructure-dependent leakage current behavior of ultrathin HfO_2 dielectrics: In situ annealing studies, Appl. Phys. Lett. 84 (12) (2004) 2064–2066, https://doi.org/10.1063/1.1667621.
[2] A.B. Mukhopadhyay, J.F. Sanza, C.B. Musgrave, Atomic layer deposition of hafnium oxide from hafnium chloride and water, 2007 Proc. - 24th Int, VLSI Multilevel Interconnect. Conf. VMIC (2007) 345–361.
[3] S. Park, B.-E. Park, H. Yoon, S. Lee, T. Nam, T. Cheon, S.-H. Kim, H. Cheon, S. Im, T. Seong, H. Kim, Comparative study on atomic layer deposition of HfO_2: Via substitution of ligand structure with cyclopentadiene, J. Mater. Chem. C. 8 (4) (2020) 1344–1352, https://doi.org/10.1039/C9TC05778A.
[4] J. Robertson, High dielectric constant gate oxides for metal oxide Si transistors, Reports, Prog. Phys. 69 (2) (2006) 327–396, https://doi.org/10.1088/0034-4885/69/2/R02.
[5] W.J. Maeng, W.H. Kim, J.H. Koo, S.J. Lim, C.S. Lee, T. Lee, H. Kim, Flatband voltage control in p-metal gate metal-oxide-semiconductor field effect transistor by insertion of TiO_2 layer, Appl. Phys. Lett. 96 (2010) 2–5, https://doi.org/10.1063/1.3330929.
[6] C. Adelmann, H. Tielens, D. Dewulf, A. Hardy, D. Pierreux, J. Swerts, E. Rosseel, X. Shi, M.K. Van Bael, J.A. Kittl, S. Van Elshocht, Atomic Layer Deposition of Gd-Doped HfO_2 Thin Films, J. Electrochem. Soc. 157 (4) (2010) G105, https://doi.org/10.1149/1.3301663.
[7] C.-H. Fu, K.-S. Chang-Liao, C.-C. Li, Z.-H. Ye, F.-M. Hsu, T.-K. Wang, Y.-J. Lee, M.-J. Tsai, A higher-k tetragonal HfO_2 formed by chlorine plasma treatment at interfacial layer for metal-oxide-semiconductor devices, Appl. Phys. Lett. 101 (3) (2012) 032105, https://doi.org/10.1063/1.4737393.
[8] J.H. Lee, I.H. Yu, S.Y. Lee, C.S. Hwang, Phase control of HfO_2-based dielectric films for higher-k materials, J. Vac. Sci. Technol. B Microelectron. Nanom. Struct. 32 (2014), https://doi.org/10.1116/1.4862952.
[9] R.I. Hegde, D.H. Triyoso, S.B. Samavedam, B.E. White, Hafnium zirconate gate dielectric for advanced gate stack applications, J. Appl. Phys. 101 (7) (2007) 074113, https://doi.org/10.1063/1.2716399.
[10] S.Y. Lee, H.K. Kim, J.H. Lee, I.-H. Yu, J.-H. Lee, C.S. Hwang, Effects of O_3 and H_2O as oxygen sources on the atomic layer deposition of HfO_2 gate dielectrics at different deposition temperatures, J. Mater. Chem. C. 2 (14) (2014) 2558–2568, https://doi.org/10.1039/C3TC32561J.
[11] Y.W. Yoo, W. Jeon, W. Lee, C.H. An, S.K. Kim, C.S. Hwang, Structure and electrical properties of Al-doped HfO_2 and ZrO_2 films grown via atomic layer deposition on Mo electrodes, ACS Appl. Mater. Interfaces. 6 (24) (2014) 22474–22482, https://doi.org/10.1021/am506525s.
[12] H.J. Cho, Y.D. Kim, D.S. Park, E. Lee, C.H. Park, J.S. Jang, K.B. Lee, H.W. Kim, Y.J. Ki, I.K. Han, Y.W. Song, New TIT capacitor with $ZrO_2/Al_2O_3/ZrO_2$ dielectrics for 60nm and below DRAMs, Solid. State. Electron. 51 (11–12) (2007) 1529–1533, https://doi.org/10.1016/j.sse.2007.09.030.
[13] D.-S. Kil, H.-S. Song, K.-J. Lee, K. Hong, J.-H. Kim, K.-S. Park, S.-J. Yeom, J.-S. Roh, N.-J. Kwak, H.-C. Sohn, J.-W. Kim, S.-W. Park, Development of New $TiN/ZrO_2/Al_2O_3/ZrO_2/TiN$ Capacitors Extendable to 45nm Generation DRAMs Replacing HfO_2 Based Dielectrics, in: 2006 Symp. VLSI Technol. 2006. Dig. Tech. Pap., IEEE, n.d.: pp. 38–39. https://doi.org/10.1109/VLSIT.2006.1705205.
[14] W. Jeon, Recent advances in the understanding of high-k dielectric materials deposited by atomic layer deposition for dynamic random-access memory capacitor applications, J. Mater. Res. 35 (7) (2020) 775–794, https://doi.org/10.1557/jmr.2019.335.
[15] M. Pešić, S. Knebel, M. Geyer, S. Schmelzer, U. Böttger, N. Kolomiiets, V. V. Afanas'ev, K. Cho, C. Jung, J. Chang, H. Lim, T. Mikolajick, U. Schroeder, Low leakage ZrO_2 based capacitors for sub 20 nm dynamic random access memory

technology nodes, J. Appl. Phys. 119 (2016), 064101. https://doi.org/10.1063/1.4941537.

[16] S.K. Kim, G.-J. Choi, S.Y. Lee, M. Seo, S.W. Lee, J.H. Han, H.-S. Ahn, S. Han, C. S. Hwang, Al-Doped TiO_2 Films with Ultralow Leakage Currents for Next Generation DRAM Capacitors, Adv. Mater. 20 (8) (2008) 1429–1435, https://doi.org/10.1002/adma.200701085.

[17] W. Jeon, S.H. Rha, W. Lee, Y.W. Yoo, C.H. An, K.H. Jung, S.K. Kim, C.S. Hwang, Controlling the Al-Doping Profile and Accompanying Electrical Properties of Rutile-Phased TiO_2 Thin Films, ACS Appl. Mater. Interfaces. 6 (10) (2014) 7910–7917, https://doi.org/10.1021/am501247u.

[18] W. Jeon, S.H. Rha, W. Lee, C.H. An, M.J. Chung, S.H. Kim, C.J. Cho, S.K. Kim, C. S. Hwang, Asymmetry in electrical properties of Al-doped TiO_2 film with respect to bias voltage, Phys. Status Solidi - Rapid Res. Lett. 9 (7) (2015) 410–413, https://doi.org/10.1002/pssr.201510146.

[19] S.W. Lee, J.H. Han, S. Han, W. Lee, J.H. Jang, M. Seo, S.K. Kim, C. Dussarrat, J. Gatineau, Y.-S. Min, C.S. Hwang, Atomic Layer Deposition of $SrTiO_3$ Thin Films with Highly Enhanced Growth Rate for Ultrahigh Density Capacitors, Chem. Mater. 23 (8) (2011) 2227–2236, https://doi.org/10.1021/cm2002572.

[20] W. Lee, J.H. Han, W. Jeon, Y.W. Yoo, S.W. Lee, S.K. Kim, C.-H. Ko, C. Lansalot-Matras, C.S. Hwang, Atomic layer deposition of $SrTiO_3$ films with cyclopentadienyl-based precursors for metal-insulator-metal capacitors, Chem. Mater. 25 (2013), https://doi.org/10.1021/cm304125e.

[21] B. Hudec, K. Hušeková, A. Tarre, J.H. Han, S. Han, A. Rosová, W. Lee, A. Kasikov, S.J. Song, J. Aarik, C.S. Hwang, K. Fröhlich, Electrical properties of TiO_2-based MIM capacitors deposited by $TiCl_4$ and TTIP based atomic layer deposition processes, Microelectron. Eng. 88 (7) (2011) 1514–1516.

[22] W. Lee, W. Jeon, C.H. An, M.J. Chung, H.J. Kim, T. Eom, S.M. George, B.K. Park, J. H. Han, C.G. Kim, T.-M. Chung, S.W. Lee, C.S. Hwang, Improved Initial Growth Behavior of SrO and $SrTiO_3$ Films Grown by Atomic Layer Deposition Using $\{Sr(demamp)(tmhd)\}_2$ as Sr-Precursor, Chem. Mater. 27 (2015), https://doi.org/10.1021/acs.chemmater.5b00843.

[23] J.M. Leger, A. Atouf, P.E. Tomaszewski, A.S. Pereira, Pressure-induced phase transitions and volume changes in HfO_2 up to 50 GPa, Phys. Rev. B. 48 (1993) 93–98, https://doi.org/10.1103/PhysRevB.48.93.

[24] X. Zhao, D. Vanderbilt, First-principles study of structural, vibrational, and lattice dielectric properties of hafnium oxide, Phys. Rev. B. 65 (2002), 233106, https://doi.org/10.1103/PhysRevB.65.233106.

[25] G.-M. Rignanese, Dielectric properties of crystalline and amorphous transition metal oxides and silicates as potential high-κ candidates: The contribution of density-functional theory, J. Phys. Condens. Matter. 17 (7) (2005) R357–R379, https://doi.org/10.1088/0953-8984/17/7/R03.

[26] C.-K. Lee, E. Cho, H.-S. Lee, C.S. Hwang, S. Han, First-principles study on doping and phase stability of HfO_2, Phys. Rev. B. 78 (2008) 1–4, https://doi.org/10.1103/physrevb.78.012102.

[27] P.R. Chalker, M. Werner, S. Romani, R.J. Potter, K. Black, H.C. Aspinall, A.C. Jones, C.Z. Zhao, S. Taylor, P.N. Heys, Permittivity enhancement of hafnium dioxide high-κ films by cerium doping, Appl. Phys. Lett. 93 (2008) 23–25, https://doi.org/10.1063/1.3023059.

[28] K. Kita, K. Kyuno, A. Toriumi, Permittivity increase of yttrium-doped HfO_2 through structural phase transformation, Appl. Phys. Lett. 86 (2005) 1–3, https://doi.org/10.1063/1.1880436.

[29] D. Fischer, A. Kersch, The effect of dopants on the dielectric constant of HfO_2 and ZrO_2 from first principles, Appl. Phys. Lett. 92 (2008) 2006–2009, https://doi.org/10.1063/1.2828696.

[30] T. Vogel, N. Kaiser, S. Petzold, E. Piros, N. Guillaume, G. Lefevre, C. Charpin-Nicolle, S. David, C. Vallee, E. Nowak, C. Trautmann, L. Alff, Defect-Induced Phase Transition in Hafnium Oxide Thin Films: Comparing Heavy Ion Irradiation and Oxygen-Engineering Effects, IEEE Trans. Nucl. Sci. 68 (8) (2021) 1542–1547, https://doi.org/10.1109/TNS.2021.3085962.

[31] G.R. Waetzig, S.W. Depner, H. Asayesh-Ardakani, N.D. Cultrara, R. Shahbazian-Yassar, S. Banerjee, Stabilizing metastable tetragonal HfO_2 using a non-hydrolytic solution-phase route: Ligand exchange as a means of controlling particle size, Chem. Sci. 7 (8) (2016) 4930–4939.

[32] H.-S. Jung, S.H. Jeon, H.K. Kim, I.-H. Yu, S.Y. Lee, J. Lee, Y.J. Chung, D.-Y. Cho, N.-I. Lee, T.J. Park, J.-H. Choi, S. Han, C.S. Hwang, The Impact of Carbon Concentration on the Crystalline Phase and Dielectric Constant of Atomic Layer Deposited HfO_2 Films on Ge Substrate, ECS J. Solid State Sci. Technol. 1 (2) (2012) N33–N37, https://doi.org/10.1149/2.020202jss.

[33] R.C. Garvie, The occurrence of metastable tetragonal zirconia as a crystallite size effect, J. Phys. Chem. 69 (4) (1965) 1238–1243, https://doi.org/10.1021/j100888a024.

[34] J. Müller, T.S. Böscke, U. Schröder, M. Reinicke, L. Oberbeck, D. Zhou, W. Weinreich, P. Kücher, M. Lemberger, L. Frey, Improved manufacturability of ZrO_2 MIM capacitors by process stabilizing HfO_2 addition, Microelectron. Eng. 86 (7–9) (2009) 1818–1821, https://doi.org/10.1016/j.mee.2009.03.076.

[35] T.S. Böscke, P.Y. Hung, P.D. Kirsch, M.A. Quevedo-Lopez, R. Ramírez-Bon, Increasing permittivity in HfZrO thin films by surface manipulation, Appl. Phys. Lett. 95 (2009) 2007–2010, https://doi.org/10.1063/1.3195623.

[36] P.K. Park, S.-W. Kang, Enhancement of dielectric constant in HfO_2 thin films by the addition of Al_2O_3, Appl. Phys. Lett. 89 (2006), 192905, https://doi.org/10.1063/1.2387126.

[37] M.M. Rahman, J.G. Kim, D.H. Kim, T.W. Kim, Characterization of Al incorporation into HfO_2 dielectric by atomic layer deposition, Micromachines. 10 (2019) 1–11, https://doi.org/10.3390/mi10060361.

[38] K. Tomida, K. Kita, A. Toriumi, Dielectric constant enhancement due to Si incorporation into HfO_2, Appl. Phys. Lett. 89 (2006) 2–5, https://doi.org/10.1063/1.2355471.

[39] S.L. Weeks, A. Pal, V.K. Narasimhan, K.A. Littau, T. Chiang, Engineering of Ferroelectric HfO_2-ZrO_2 Nanolaminates, ACS Appl. Mater. Interfaces. 9 (15) (2017) 13440–13447, https://doi.org/10.1021/acsami.7b0077610.1021/acsami.7b00776.s001.

[40] L. Tang, H. Maruyama, T. Han, J.C. Nino, Y. Chen, D. Zhang, Resistive switching in atomic layer deposited HfO_2/ZrO_2 nanolayer stacks, Appl. Surf. Sci. 515 (2020) 146015, https://doi.org/10.1016/j.apsusc.2020.146015.

[41] W. Zheng, K.H. Bowen, J. Li, I. Dabkowska, M. Gutowski, Electronic structure differences in ZrO_2 vs HfO_2, J. Phys. Chem. A. 109 (2005) 11521–11525. https://doi.org/10.1021/jp053593e.

[42] Y. Lee, W. Jeon, Y. Cho, M.H. Lee, S.J. Jeong, J. Park, S. Park, Mesostructured $Hf_xAl_yO_2$ Thin Films as Reliable and Robust Gate Dielectrics with Tunable Dielectric Constants for High-Performance Graphene-Based Transistors, ACS Nano 10 (2016) 6659–6666. https://doi.org/10.1021/acsnano.6b01734.

[43] J.S. Lee, W.H. Kim, I.K. Oh, M.K. Kim, G. Lee, C.W. Lee, J. Park, C. Lansalot-Matras, W. Noh, H. Kim, Atomic layer deposition of Y_2O_3 and yttrium-doped HfO_2 using a newly synthesized $Y(iPrCp)_2(N\text{-}iPr\text{-}amd)$ precursor for a high permittivity gate dielectric, Appl. Surf. Sci. 297 (2014) 16–21, https://doi.org/10.1016/j.apsusc.2014.01.032.

[44] T.S. Böscke, S. Govindarajan, P.D. Kirsch, P.Y. Hung, C. Krug, B.H. Lee, J. Heitmann, U. Schröder, G. Pant, B.E. Gnade, W.H. Krautschneider, Stabilization of higher-κ tetragonal HfO_2 by SiO_2 admixture enabling thermally stable metal-insulator-metal capacitors, Appl. Phys. Lett. 91 (2007) 89–92, https://doi.org/10.1063/1.2771376.